Are hypervelocity impacts able to produce chondrule-like ejecta?

Clément Ganino, Guy Libourel, Akiko Nakamura, Patrick Michel

Are hypervelocity impacts able to produce chondrule-like ejecta?

Clément Ganino[1*], Guy Libourel[2,3], Akiko M. Nakamura[4], Patrick Michel[2]

[1]Université Côte d'Azur, OCA, CNRS, Géoazur, 250 rue Albert Einstein, Sophia-Antipolis, 06560 Valbonne, France.

[2]Université Côte d'Azur, OCA, CNRS, Lagrange, Boulevard de l'Observatoire, CS 34229, 06304 Nice Cedex 4, France.

[3]Hawai'i Institute of Geophysics and Planetology, School of Ocean, Earth Science and Technology, University of Hawai'i at Mānoa, Honolulu, Hawai'i 96821, USA.

[4]Graduate School of Science, Kobe University, 1-1 Rokkoudai-cho, Nada-ku, Kobe, 657-8501, Japan.

*corresponding author. Email: ganino@unice.fr

Abstract

Chondrules are one of the major components of primitive meteorites. Their sphericity indicates they formed as molten fragments or droplets but conditions and mechanisms of chondrule formation remain unknown. A possible scenario is their formation during hypervelocity impacts and ejections. To challenge this idea, we prepared an experiment that reproduces analogous of iron metal -rich chondrules by impact between a glassy silicate projectile and a metallic steel target. The hypervelocity experiment setting allowed an impact velocity of 5 km/s, and was also designed to collect the ejecta. A scanning electron microscopy survey shows that silicate ejecta share several similarities with chondrules. They formed from a population of small melt fragments whose size distribution has the same shape as the size distribution of chondrules, with a shift in size: ejecta are about one order of

magnitude smaller than typical chondrules ($\log(d_{chondrules}/d_{ejecta}) = 1.3^{+0.5}_{-0.7}$). We attribute this difference in size to the large discrepancy in the size of the impactors (only small 3 mm particle in our experiment versus km-scale planetesimal expected in an impact forming scenario for chondrules). The silicate ejecta formed in the ejecta plume contains numerous small size spherical iron metal beads. Such beads are also observed in numerous chondrules of CO chondrites specifically presented here but also documented in L and LL ordinary chondrites. Size distributions of metal beads in ejecta and chondrules of a carbonaceous chondrite used as reference material (Yamato 81020 CO) display a same shape but with a size shift, quite similar to the one observed between the ejecta droplets and the chondrules: the diameter of metal beads in ejecta is about one order of magnitude smaller than the diameter of the ejecta themselves ($\log(d_{ejecta}/d_{metal\ beads\ in\ ejecta}) = 1.2^{+0.9}_{-0.8}$), and the diameter of metal beads in chondrules is about one order of magnitude smaller than the diameter of the chondrules themselves ($\log(d_{chondrules}/d_{metal\ beads\ in\ chondrules}) = 1.4^{+0.6}_{-1.0}$). We attribute this size differences to the blast dynamics: for a same velocity and surface tension, fragments of silicate liquid will be stable when iron liquid fragments of similar size will be separated into smaller droplets. In our experiment, the biggest iron metal beads (~7 µm) are within the mean size range of silicate ejecta and can be considered as analogous of the rare large rounded metallic grains (nearly the same size as chondrules) documented in CB chondrites. The textural analogies exposed here provide support for a production of chondrules by impact.

1. Introduction

Chondrites, the most primitive meteorites, are considered as the main building block of early planetesimals (e.g. Scott, 2007) and are composed in various proportion – up to 80 vol% for ordinary chondrites (Jones et al., 2002) – of chondrules. Chondrules are spherules largely consisting of the silicate minerals olivine and pyroxene formed at high temperatures as

dispersed molten droplets that likely contain much important information on the processes of the planetary formation.

Chondrules size distribution is generally quite homogeneous (0.1 to 2 mm in diameter; e.g. Teitler et al., 2010). The size distribution of chondrules is typically determined by disaggregation (e.g. Cuzzi et al., 2001), a method that may undercount very small and/or relatively friable chondrule types, and by thin section measurements (e.g. Eisenhour, 1996), a method that requires corrections of the measured size distribution to estimate "true" three-dimensional grain sizes from random two-dimensional sections. These technics are not accurate in counting very small "microchondrules" (5-40 μm in diameter), found in the matrix or in rare clasts in at least a few chondrites, and "megachondrules" (>1 cm in diameter), discovered as fragments (Nagahara, 1984; Rubin et al., 1982; Ruzicka et al., 1998). Chondrule sizes and masses in various samples have been described as following lognormal (King and King, 1979), Rosin or Weibull distributions (Eisenhour, 1996; Hughes, 1978a, 1978b) even if Teitler et al. (Teitler et al., 2010) explained that for some chondrule data sets, lognormal or Weibull functions are statistically not good fits of the size distribution. Nevertheless, the size distribution displays a non-zero minimum chondrule size, typically about 10-20% of the mean size (Eisenhour, 1996). Each chemical group of chondrite possesses a distinct size-frequency distribution of chondrules. The mean size is quite uniform with ordinary chondrites (L, LL) having the largest, carbonaceous chondrite from Mighei and Ornans groups (CM and CO) having lower average size (King and King, 1978) and carbonaceous chondrite with high metal content (CH) displaying even lower size (e.g. Grossman et al., 1988; Scott, 1988).

The process responsible for the formation of chondrules is still a matter of debate and it is even not established if a unique or multiple distinct processes are required to form chondrules. The igneous textures of chondrules indicate that they were produced by melting

and solidification in the early solar nebula (e.g. Scott, 2007). There are several hypothesis proposed, including the formation of chondrules by planetesimal collisions (Johnson et al., 2018, 2015; Johnson and Melosh, 2014; Urey, 1952), by splashing molten planetesimals where energy for melting is radioactivity (e.g. Asphaug et al., 2011; Sanders and Scott, 2018), by shock waves (Connolly and Love, 1998; Morris and Boley, 2018) or other processes including for instance X-wind model (Shu et al., 1996), lightning (Pilipp et al., 1998), radiant heating by magma ocean (Herbst and Greenwood, 2016), or localized magnetized dissipation (Joung et al., 2004).

Krot et al. (2014, 2005) demonstrated that at least some of the latest (~5 Ma post-Calcium-Aluminium-rich Inclusions (CAI), the oldest substances in the Solar System) iron-rich chondrules from Carbonaceous Bencubbin-type (CB) and Carbonaceous "High-metal" chondrites (CH) formed by impact. An impact origin is clearly established, in this particular case, and the chondrules and metal grains in the CB chondrites would have formed from a vapor–melt plume produced by a catastrophic disruption between planetary embryos. The remaining question is whether most chondrules are derived from disrupted planetesimals or if CB and CH are exceptions. In other chondrite groups, as in L, LL or CO, chondrules frequently contain iron-nickel metal spherules, distributed in their interiors and/or located at their surface. Where the metal is located at the surface of the chondrules, the shape is not spherical (e.g. Uesugi et al., 2008) and the metal forms an asymmetric globule. In most other cases where the metal beads are inside the chondrules, the shape is spherical. Such spherical shape of both chondrules and metal beads is an evidence for a liquid behavior before their solidification (Rambaldi and Wasson, 1981; Skinner and Leenhouts, 1993; Wang et al., 2007) that requires the presence of two distinct and immiscible molten phases.

Our objective here was to perform a hypervelocity impact experiment to investigate the textural properties of ejected material and to compare to the textural properties of iron

metal beads bearing chondrules. Here we aimed at performing impact at a velocity close to that expected in the main asteroid belt (Bottke Jr et al., 1994) and a possible order of magnitude of impact velocity in the protoplanetary disk (~ 5.3 km/s). Is it possible to reproduce chondrule-like objects by shooting a silicate projectile into an iron metal target? Is the mechanical process that create a contrasted distribution of metal and silicate liquid droplets in chondrule acting in the hypervelocity impact experiment? This study will help to discuss some physical properties of the spray produced during an impact and the possibility that such chondrules formed from impact during the early Solar System history.

2. Experimental setup

2.1. The impact experiment

Impact experiment was conducted using a two-stage light-gas gun at Institute of Space and Astronautical Science (ISAS), Japan, where projectile can be accelerated at the impact velocity up to ~7 km/s, which is comparable to typical asteroid-belt collisional velocity (5.3 km/s; Bottke et al., 1994). The projectile was a dunite cylinder, 0.074 g in mass, 3.2 mm in diameter and 3 mm in thickness. The measured impact velocity (4.909 km/s) was close to the one we planned (5 km/s). The target was a steel cylinder used in a previous study (Ganino et al., 2018). The chamber was evacuated to 3 Pa. The trajectory of the projectile and ejecta was captured by a high-speed video camera (Shimazu HPV-X). The camera was operated with frame interval of 2 μs with 0.5 μs exposure and the spatial resolution is about 0.3 mm/pixel. The ejecta plume contains thousands of ejecta that were collected on aluminum witness plates used as “ejecta catchers” (Figure 1). As this unique shoot provides thousands of ejecta to characterize we limited our statistical analysis to one experiment.

2.2. Imaging and analyzing major elements using SEM(-EDX)

The analyses of the ejecta was performed using the Scanning Electron Microscope Philipps FEI XL30 ESEM LaB6 equipped with a BRUKER Quantax 655 detector, operated at 20 kV and 200 nA beam current at CEMEF-Mines ParisTech.

2.3. Particle size distribution determination

The contrasted composition of the iron-rich ejecta, the aluminum plates used as ejecta catcher and the SiO_2 –rich ejecta measured using Energy-dispersive X-ray spectroscopy (Ganino et al., 2018) resulted in contrasted gray level on the backscattered electron image (Figure 2), allowing a convenient detection and identification. We used the particle analyser tool of ImageJ software to count and measure the size distribution of both the SiO_2 ejecta and the metal beads contained within the ejecta.

In this article we call melt "fragments" or melt "droplets" the molten material, droplets being the result of break-up of fragments following Johnson and Melosh (Johnson and Melosh, 2014), and "beads" the spherical solidified material (e.g., metal spherules in chondrules or in ejecta). As we wanted to estimate the size of the melt fragments and droplets produced during the impact rather than that of the flattened "splashed" ejecta on the aluminum plate, we measured the surface and estimated the volume of observed splashed ejecta and recalculated the diameter of an equivalent sphere. Assumption for this calculation is that most splashed ejecta were 1 µm- thick as inferred from tilted SEM image of the ejecta catcher. 9326 ejecta were measured. Thirteen ejecta were randomly chosen and focused on for determination of the size distribution of the 1625 metal beads they contained. These thirteen ejecta display a large scale range (Figure 2).

2.4. Distribution of metal beads in chondrules

The presence of metal beads in chondrules is well known, but their size distribution is not documented and their abundance largely differs from a chondrite family to another (Scott and Krot, 2003). We used back-scattered electron image of the carbonaceous chondrite

Yamato 81020 (CO 3.0) (Figure 3) to describe the size distribution of metal beads. Yamato 81020 is a perfect sample for this study because it is a primitive object (carbonaceous chondrite, see Libourel et al, 2017) poorly altered (no sulfidation, etc), and it is a metal rich-chondrite with abundant metal beads in the large majority of its chondrules. In the same way to the procedure that we used to determine the size distribution of the ejecta in the experiment, we used the particle analyser tool of ImageJ software to count and measure the 2D-size distribution of metal beads contained within the chondrules of Yamato 81020. Here, the data are apparent diameters measured on a two-dimensional surface and include sections of metal beads. When the sample is sectioned, not all particles/grains are sectioned through their maximum diameter, many appear smaller than they actually are. The size distribution is therefore, inherently biased to smaller sizes. The measured size distribution can be corrected with a stereological analysis. We used, a classical Saltykov analysis (Saltykov, 1958) also called "Schwartz-Saltykov", that allows to compute a statistical equivalent 3D size distribution from a 2D size distribution considering that the grains are represented by their equivalent spheres.

3. Results

3.1. Chondrule size distribution in CO chondrites

CO chondrites have different types of chondrules, some of which are non-spherical and present a wide range of shapes (Figure 3). Rubin and Wasson (2005) show that some chondrules in Yamato 81020 are multi-lobate or distended or highly irregular in two dimensions. The circular chondrules are moderately equant with aspect ratios in thin section varying from 1.02 to 1.11.

The size-frequency distribution of 2834 chondrules in CO chondrites was determined by petrographic analysis of thin sections by Rubin (1989). The data are not corrected and

apparent diameters were measured on a two-dimensional surface and display a mean of 148^{+132}_{-70} μm. We used the initial two dimensional chondrule size distribution of Rubin (Rubin, 1989) transformed into a theoretical three dimensional size distribution after a Saltykov analysis (Saltykov, 1958).

The chondrule theoretical three-dimensional size distribution best fit is a Rosin distribution (Hughes, 1978a) expressed as

$$ch\% = 100 * \left(1 - e^{-bd^n}\right) \quad (1)$$

where *ch%* is the percentage of chondrules, *d* is the diameter in micron and *b* and *n* are constants and are parameters of the distribution (respectively *1/b* being the scale parameter and *n* being the shape parameter). For our best fit, *b* = -2.60 and *n* = 1.13. The correlation coefficient of the linear regression in the plot log(-ln(1-*ch%*) = f(log(*d*)) is very good (*r* = -0.96). Following the results from Hughes (Hughes, 1978a) a better correlation (*r* = 0.99) is obtained using a 3 parameters Weibull law distribution expressed as

$$ch\% = 100 * \left(1 - e^{-b(d-\gamma)^n}\right) \quad (2)$$

where γ is the location parameter and with best fit for $\gamma = 131$ μm, *b* = -1.35 and *n* = 0.74. The excellent correlation coefficients demonstrate we are in the case where Rosin and three parameters Weibull laws fit the dataset as very often for chondrules (Hughes, 1978a; Teitler et al., 2010).

3.2. Silicate ejecta size distribution in high velocity impact plume

Ejecta we collected appear as stuck patches on the ejecta catcher with a nearly circular shape, a typical thickness of 1 µm and an apparent diameter that largely varies from 3.7 µm to 61.2 µm. As all ejecta present a circular shape, we infer they were all formed from splashing melt fragments and droplets.

Despite the relatively low impact energy due to the small size of the projectile, our impact experiment provides abundant melted material. In fact, a precise quantification is not straightforward, but at a first glance, most ejecta have rounded shapes and result from solidification of molten material whereas only rare, always metallic, fragments are angular and could be remnants of unmolten pieces of the target. Because of the exposure duration of the high velocity camera (0.5 µs), the ejecta particles with a velocity of 5 km/s moved of ~2.5 mm during the exposure. In other words, the ejecta particles appear by 2.5 mm longer than they are. Moreover, the spatial resolution of the camera was not sufficient (>0.3 mm/pixel) to determine the size distribution of ejected material during the flight. Therefore, what we can observe on the images (Figure 1) are only slow (< km/s) and relatively large (> mm) fragments. To characterize the ejecta population, we use the ejecta catcher. Our experimental setting was not appropriate to sample the whole plume of ejecta, but we find only rare angular fragments, generally of iron-metal (from the target) and relatively large (>100µm) that were ejected during the impact. The remaining ejecta collected on the aluminum plate have a rounded shape compatible with a pronounced melting of silicate (from the projectile) and metal (from the target) material.

The size of the silicate ejecta recovered on the ejecta catcher and that come from the major mass of the ejecta plume is related to fragments and droplets with a diameter in the range ~4-17 µm (mean = 7.87 µm, median = $6.43^{+10.31}_{-2.49}$ µm; the confidence interval calculated to include 90% of the sample data within). The size distribution of the ejecta is very similar in shape with the size distribution of chondrules (Figure 4) and fits a Rosin distribution as in equation (1). In our best fit for the size distribution of silicate ejecta, b = -0.88 and n = 1.04. The correlation coefficient of the linear regression in the plot log(-ln(1-*ej%*) = f(log(*d*)) where *ej%* is the percentage of ejecta and *d* the diameter is very good

(r = 0.97). Here again, a better correlation (r = 0.99) is obtained using a three-parameters Weibull law with $\gamma = 5.3\ \mu m$, b = -0.17 and n = 0.62.

3.3. Metal beads size distribution in ejecta and chondrules of Yamato 81020 (CO 3.0)

The silicate ejecta formed in the ejecta plume contains numerous small size (mostly <1 µm) spherical iron metal beads (Figure 2). Metal beads were observed and measured in 13 randomly chosen ejecta. All beads are in the range 0.07-7.0 µm with a mean size of 0.55 µm and a median of $0.40^{+0.99}_{-0.26}$ µm. The size distribution was plotted for the independently analyzed ejecta (thin dotted-lines in Figure 4d) and for the sum of all beads (1625 beads) in that 13 ejecta (thick dotted-line in Figure 4d). The distribution follows a Rosin size distribution (r = 0.98) with b = 0.36 and n = 0.55 or a three-parameter Weibull distribution (r = 0.99) with $\gamma = 0.53\ \mu m$, b = 0.50 and n = 0.36.

Even if they are generally much larger (up to few tens of micrometers), such spherical metal beads are very frequent in chondrules of the carbonaceous chondrite Yamato 81020 (CO 3.0). In that meteorite, many chondrules contain metal bead. We observed and measured the size of metal beads in nine randomly chosen chondrules from Yamato 81020. From the two-dimensional size distribution, we calculated the theoretical three-dimensional size distribution after a Saltykov analysis (Saltykov, 1958). Their diameter range is 2.1 – 81.1 µm with a mean of 9.38 µm and a median of $5.65^{+23.00}_{-3.21}$ µm. Here again, the size distribution was plotted for the independently analyzed chondrules (thin dotted-lines in Figure 4c) and for the sum of all beads (3517 beads) in that 9 chondrules (thick dotted-line in Figure 4c). The distribution follows with an excellent fit (r = 0.99) a Rosin size distribution with b = -0.77 and n = 0.95 or a three-parameter Weibull distribution (r = 0.99) with $\gamma = 4.71\ \mu m$, b = -0.44 and n = 0.77.

4. Discussion

4.1. Size of chondrules, metal beads and ejecta

Distinct size-frequency chondrule distributions made some authors propose a sorting mechanism, as for instance aerodynamic drag (Dodd, 1976; Shu et al., 1996). Following the idea of an impact origin for chondrules, their mean size would then be explained by the solidification of ejected melt fragments and droplets produced by impactors <10 km in diameter (Benoit et al., 1999; Melosh and Vickery, 1991).

The textural homogeneity observed in our ejecta and chondrules, with silicate and metal droplets having similar pattern of size distribution, suggests that material experienced mechanical sorting. The particles might have been size-sorted under virtually identical conditions and following a similar physical process. The material initially shocked to high pressure could have approached the liquid-vapor phase boundary from the liquid side during decompression: the formation of a condensate layer formed from a gas phase during the experiment was documented by Ganino et al. (Ganino et al., 2018). The decompression caused the break-up into an expanding spray of melt fragments and droplets of the ejecta blast. Following Melosh and Vickery (Melosh and Vickery, 1991), the equilibrium droplet radius (R) depends on the size of the impactor (L) and the impact velocity (v_{imp}) following the equation

$$R = 0.11 \frac{\sqrt{L}}{v_{imp}} \quad (3)$$

With this model, mean size of chondrules would then be explained by the solidification of ejected melt fragments produced by impactors <10 km in diameter (Benoit et al., 1999). When we apply this equation to the ejecta produced during the hypervelocity experiment, we find that expected radius for a 3 mm impactor shot at 4.909 km/s is about 1.2 µm, equivalent

to a diameter of ~2.4 µm. This estimate is too small compared to what we observed. Melosh and Vickery (Melosh and Vickery, 1991) modeling corresponds to melt ejection as a half sphere expanding into free space, a geometry that closely represents the geometry of a vapor plume, while the ejecta plume in our experiment presents a significantly different geometry (Figure 1). Johnson and Melosh (Johnson and Melosh, 2014) performed impact simulations using the hydrocode modelling iSALE to constrain the properties of the ejecta curtain. To calculate the size (diameter) of ejected melt fragments as a function of ejection velocity, impact velocity, and impactor size they proposed the following equation (Johnson and Melosh, 2014),

$$d_{fragments} \sim 0.14 \left(\frac{v_{ej}}{v_{imp}}\right)^{-0.81} \left(\frac{R_{imp}}{v_{imp}}\right)^{\frac{2}{3}} \quad (4)$$

When analyzing the high-speed video images, the leading edge of the ejecta cloud had velocity of ~4.6 km/s corresponding to an estimate of the ejection velocity used in equation (4). With this value, the theoretical size of melt fragments calculated from Johnson and Melosh (Johnson and Melosh, 2014) equation would be $d_{\text{fragments}}$ = 6.69 µm. The expected diameter for melt fragment is close to the mean diameter of the ejecta we observed (mean = 7.87 µm, median = $6.43^{+10.31}_{-2.49}$ µm) making us propose that the physical process described in this equation could explain the observations from our experiment. In the post-impact blast, when fragmentation occurs in the ejecta plume, ejected melt fragments can be accelerated by aerodynamic drag as the surrounding vapor flows past the melt. The balance of the aerodynamic drag force and surface tension determines the size of the melt droplets. In that case, the size of the ejecta we collected and measured on the ejecta-catcher depends on the size of the melt fragments in the impact plume that might be governed by the balance between the surface tension and relative kinetic energy. Johnson and Melosh (Johnson and Melosh, 2014), argued that melt "droplets" also form during the blast, as a result of break-up

of larger melt fragments and proposed an equation to estimate the size (diameter) of melt droplets:

$$d_{droplets} \sim 0.025 \left(\frac{v_{ej}}{v_{imp}}\right)^{-0.97} {R_{imp}}^{\frac{1}{2}} {v_{imp}}^{-1} \qquad (5)$$

For our experiment, the theoretical diameter of melt droplets calculated from Johnson and Melosh (Johnson and Melosh, 2014) equation would be $d_{droplets}$ = 0.21 µm. This size is clearly too low to explain the observed size distribution of silicate ejecta. Nevertheless, it is close to the order of magnitude of the diameter of the metal beads found in the ejecta (mean = 0.55; median = $0.40^{+0.99}_{-0.26}$ µm) that could be explained, following Johnson and Melosh (Johnson and Melosh, 2014) process, by the break-up of larger melt fragments of metal.

In our quantitative study, the difference between the size of chondrules in CO, the size of ejecta in hypervelocity experiment and the sizes of metal beads in chondrules and in ejecta can be obtained quantifying the horizontal shift between the distribution curves (Figure 5): the diameter of metal beads in ejecta is ~ 1.2 order of magnitude smaller than the diameter of the ejecta themselves ($\log(d_{ejecta}/d_{metal\ beads\ in\ ejecta}) = 1.2^{+0.9}_{-0.8}$), and the diameter of metal beads in chondrules is ~ 1.4 magnitude smaller than the diameter of the chondrules themselves ($\log(d_{chondrules}/d_{metal\ beads\ in\ chondrules}) = 1.4^{+0.6}_{-1.0}$). These results can also be deduced from the 3 parameters Weibull law distributions we obtained for our data. The shape parameter (n) is very close for all distribution ($n_{chondrules}$ = 0.74; n_{ejecta} = 0.62; $n_{beads\ in\ chondrules}$ = 0.77; $n_{beads\ in\ ejecta}$ = 0.36), and if we focused on the location parameter (γ), we confirm that there is a one order of magnitude shift between the diameter of chondrules and the diameter of metal beads in chondrules ($\log\left(\gamma_{chondrules}/\gamma_{metal\ beads\ in\ chondrules}\right) = 1.4$) and between the diameter of ejecta and the diameter of metal beads in ejecta ($\log\left(\gamma_{ejecta}/\gamma_{metal\ beads\ in\ ejecta}\right) = 1$).

That discrepancy would suggest that the physical process that created a contrasted distribution of metal beads and silicated chondrules in chondrites might govern similar distributions in the hypervelocity impact experiment. The process proposed by Johnson and Melosh (Johnson and Melosh, 2014) could explains the contrasted size between silicate ejecta and metal beads :it would be related to the break-up of melt fragments into smaller melt droplets that would occur for metal melt but not for silicate melt. A way to analyze the flow regime in a multiphase fluid flows is to calculate the Weber number (We). This dimensionless parameter is defined as the ratio of the momentum in the vapor layer divided by the surface tension force restraining the liquid following the equation

$$We = \frac{\rho {v_f}^2 l}{\sigma} \quad (6)$$

where ρ is the density of the fluid, v_f is its velocity, l is its characteristic length, for instance the droplet diameter and σ is the surface tension. There is a critical Weber number (We_c) above which drop break-up occurs. This critical number depends on the fluid properties but is generally close to 12 (e.g. Pilch and Erdman, 1987). In our experiment during the post-impact blast illustrated by Figure 1, the ejecta were propelled as high velocity relatively thick filaments (Figure 1 and Ganino et al., 2018). The intricate non-spherical shapes of the filaments show that the Weber number (We) for the fluid flow is high and should drive a first break-up into small spherical fragments by sheet stripping (Chigier and Reitz, 1996). Density being higher in iron liquid than in silicate liquid, for a same velocity and surface tension, fragments of silicate liquid will be stable ($We_{\text{silicate melt fragments}} < We_{\text{critical}}$) when iron liquid fragments of similar size will be separated by a second break-up from “melt fragments” to “melt droplets” ($We_{\text{iron melt fragments}} > We_{\text{critical}}$). If this scenario of droplets formation by sheet stripping is true, the size sorting between the silicate droplet and the smaller metal droplet

would be acting and efficient in an extremely short scale (the flight length is about10 cm) and timescale (the flight duration is few tens of µs).

These results could explain the mean size of metal beads versus silicate ejecta or chondrules. If we now look at the extreme values, i.e. the biggest metal beads produced during the experiment (size = 7.0 µm), it is of note that they are very close to the mean and median size of silicate ejecta (mean = 7.87 µm, median = $6.43^{+10.31}_{-2.49}$ µm). The largest metal beads in our experiment would derived from melt fragments of metal that did not break-up into smaller melt droplets. A possible explanation would be that their We number was too low ($We_{\text{iron melt fragments}} < We_{\text{critical}}$), and it could be the case if these melt fragments were ejected with a velocity below the average, or if their temperature was slightly different, resulting in distinct surface tension, We number, and mechanical behavior during the blast. In a planetary perspective, large metal beads with a diameter close to the typical diameter of chondrules are also documented and are also relatively rare. Large metal beads are described in some chondrites where their size range is similar to the size of chondrules, as for instance the "large" metallic grains found in CB (Krot et al., 2005).

4.2. Origin of the metal beads in chondrules

In natural samples, as in Yamato 81020, not all chondrules display abundant iron-metal beads (see also Libourel and Portail, 2018). An explanation could be that all chondrules initially contained iron droplets, but separation operated to various degrees between melted iron globules and melted chondrules (Uesugi et al., 2008). Size sorting of metal and silicate fractions might suggest that sorting of metallic beads is linked to a certain extent to the siderophile depletion in chondrites (following Skinner and Leenhouts, 1993).

Another explanation would be that the iron-bead content is directly related to the elementary abundance of iron that may strongly differ from one chondrule to another. In the

370 case chondrules were formed by impact, the chemical composition of the planetary bodies
371 involved in the impact are of first importance: impact involving iron-rich differentiated bodies
372 would involve larger volume of metal-rich ejecta. With our experimental setting, it is clear
373 that a significant proportion of metal beads may be molten fragments of the steel target
374 (Ganino et al., 2018). The processes of projectile–target interaction and inter-element
375 fractionation during and immediately after the impact process are now well documented (e.g.
376 Ebert et al., 2013; Evans et al., 1994; Hamann et al., 2013; Mittlefehldt et al., 2005, 1992).
377 Nevertheless, another process could be involved in the occurrence of iron-metal, as the high
378 temperature reached during the impact may cause the reduction of FeO contained in the
379 silicate projectiles into iron metal following the reaction:

380 $$FeO_{(silicate\ liquid)} = Fe_{(metal\ liquid)} + ½\ O_{2(gas)} \quad (7)$$

381 Shock induced in-situ reduction of FeO is well known during hypervelocity and
382 impact experiments (Ganino et al., 2018; Rowan and Ahrens, 1994) and examples are
383 described in natural craters on Earth where iron metal spheres are also observed disseminated
384 in silicate impact melt (e.g., Meteor Crater and Wabar craters, respectively, described by
385 Mittlefehldt et al., 2005 and Hamann et al., 2013).

386 Hypervelocity impact experiment carried out in this study provides further support to
387 an impact forming scenario for chondrule formation: similarly, in catastrophic disruption
388 between large bodies, immiscibility may occur between the silicate and iron liquids – the
389 latter forming from iron metal initially present in the colliding bodies or forming from FeO
390 reduction when the temperature rises.

391 In this article, we underlined the remarkable analogies between chondrules size
392 distribution in CO carbonaceous chondrites and ejecta formed in the hypervelocity
393 experiment. We also mentioned the striking analogies in their metal-beads contents, following
394 the idea that a similar sorting mechanism could act. Important aspects remain to be discussed

as the other proxies we can use to challenge such scenario and the possible chronology in the early history of the Solar System. The thermal history of chondrules brings constraints that could help to discriminate between chondrule formation models (Jones et al., 2018). Porphyritic textures are produced when a chondrule is heated to a maximum temperature close to its liquidus (typically 1400 to 1700°C), and cooled at initial rates between about 10 and 1,000 °C/h. Nonporphyritic chondrules develop when peak temperatures exceed the liquidus and chondrules cool at rates around 500–3,000 °C/h. In our experiment, ejecta remain glassy; such conditions being closed to those of hyper-quench (cooling rate of several 10^5-10^6 °C.s^{-1}). What would be expected in larger ejecta blast? A modelling of the radiative cooling of a ballistically expanding spherical cloud of chondrule droplets ejected from the impact site is proposed by Dullemond et al. (2014). This article confirm its compatibility with the cooling history of chondrules inferred from the texture, and mineral composition (Jones et al., 2018). Radiative cooling of a droplet cloud produces cooling rates that can be related not only to the different types of texture of the chondrules but also to their relative abundance (Delpeyrat et al., 2019). Focusing on jetted material, Johnson et al. (Johnson et al., 2015) demonstrated that melted droplets jetted during large-scale accretionary impacts would also exhibit the observed igneous textures of chondrules. In a chondrule forming process associated to impact involving molten planetesimals (Asphaug et al., 2011) the cooling rate, limited by opacity, is regulated by the expansion timescale and depends on local swarm density and proximity to the boundary. In this case, chondrules can be used as proxy to constrain the swarm dynamics.

Nevertheless, the formation of chondrules from large impact questions the early evolution of the Solar System: chondrule formation would occur when planetesimals and their collisions were abundant and it is generally believed that planetesimals would only accrete once chondrules formed. A support to this scenario, that seems contradictory at a first glance,

comes from isotopic analyses of magmatic iron meteorites (Kruijer et al., 2014). These analyses bring support to a possible synchronicity of planetesimal and chondrules formation, showing that the parent bodies of magmatic iron meteorites greater than 10–100 km in diameter could have accreted ~0.1–0.3 Myr after the formation of CAIs. With a such age, some planetesimals would have formed before most chondrules and chondrites would not be the direct primitive accreting blocks of that planetesimals, but a consequence of their accretion.

Conclusion

The hypervelocity experiment presented here, involving a silicate projectile on an iron metal target, produces ejecta that share several similarities with metal beads rich chondrules. These ejecta appear as largely molten splashed ejecta sampled on a screen, coming from a population of small melt fragments and droplets. The size distribution of the ejecta is similar to the size distribution of chondrules in CO chondrites, with a shift in size. The ejecta were about an order of magnitude smaller than CO chondrules, a result that is expected by the fact that the equilibrium melt fragments size depends on is the size of the impactor (small 3 mm particle in our experiment versus km-scale planetesimal in an impact forming scenario for chondrules). The silicate ejecta formed in the ejecta plume contains numerous small size spherical iron metal beads as consistent with what is frequently observed in chondrules. The biggest iron metal droplets (~7µm) fall in the size mean size range of silicate ejecta and could be considered as analogous of large (same size as chondrules) rounded metallic grains documented in CB chondrites. The size distributions of metal beads in ejecta and chondrules are similar but with a size shift: iron-metal beads in the ejecta are about an order of magnitude smaller than iron-metal beads in the chondrule of Yamato 81020. We attribute the difference in mean size between silicate melt (chondrule or ejecta) and metal melt (beads in chondrules

or beads in ejecta), to the break-up from melt "fragments" to melt "droplets". This process would be efficient for metal melt but not for silicate melt because of their different density (higher in iron liquid than in silicate liquid). For a same velocity and surface tension, fragments of silicate liquid were stable when iron liquid fragments of similar size were separated. The remarkable textural analogies between chondrules and ejecta exposed here give support for a production of chondrules during impact, implying that chondrites would not be the direct primitive accreting blocks of the planets, but a byproduct of their accretion.

Acknowledgements

The authors acknowledge two anonymous reviewers for their corrections and comments that greatly improved this article. CG thanks Suzanne Jacomet, Olivier Tottereau and Jean Furstoss. This project was supported by Programme National de Planétologie (PNP) - Institut National des Sciences de l'Univers (INSU), by Université Côte d'Azur-IDEX-Académie 3, and by BQR from Observatoire de la Côte d'Azur (OCA); GL thanks Centre National d'Etudes Spatiales (CNES) and Fondation Doeblin; AN thanks to the Hypervelocity Impact Facility (former facility name, The Space Plasma Laboratory), Institute of Space and Astronautical Science (ISAS), and Japan Aerospace Exploration Agency (JAXA) for their support. PM thanks CNES.

References

Asphaug, E.I., Jutzi, M., Movshovitz, N., 2011. Chondrule formation during planetesimal accretion. Earth Planet. Sci. Lett. https://doi.org/10.1016/j.epsl.2011.06.007

Benoit, P.H., Symes, S.J.K., Sears, D.W.G., 1999. Chondrule size distributions: What does it

mean?, in: Lunar and Planetary Science Conference.

Bottke Jr, W.F., Nolan, M.C., Greenberg, R., Kolvoord, R.A., 1994. Velocity distributions among colliding asteroids. Icarus 107, 255–268.

Chigier, N., Reitz, R.D., 1996. Regimes of jet breakup and breakup mechanisms- Physical aspects. Recent Adv. spray Combust. Spray At. drop Burn. phenomena. 1, 109–135.

Connolly, H.C., Love, S.G., 1998. The formation of chondrules: Petrologic tests of the shock wave model. Science (80-.). 280, 62–67.

Cuzzi, J.N., Hogan, R.C., Paque, J.M., Dobrovolskis, A.R., 2001. Size-selective concentration of chondrules and other small particles in protoplanetary nebula turbulence. Astrophys. J. 546, 496.

Delpeyrat, J., Pigeonneau, F., Libourel, G., 2019. Chondrule radiative cooling in a non-uniform density environment. Icarus.

Dodd, R.T., 1976. Accretion of the ordinary chondrites. Earth Planet. Sci. Lett. 30, 281–291.

Dullemond, C.P., Stammler, S.M., Johansen, A., 2014. Forming chondrules in impact splashes. I. radiative cooling model. Astrophys. J. https://doi.org/10.1088/0004-637X/794/1/91

Ebert, M., Hecht, L., Deutsch, A., Kenkmann, T., 2013. Chemical modification of projectile residues and target material in a MEMIN cratering experiment. Meteorit. Planet. Sci. https://doi.org/10.1109/ICCA.2014.6870956

Eisenhour, D.D., 1996. Determining chondrule size distributions from thin-section measurements. Meteorit. Planet. Sci. 31, 243–248.

Evans, N.J., Shahinpoor, M., Ahrens, T.J., 1994. Hypervelocity impact: Ejecta velocity, angle, and composition. Large Meteor. Impacts Planet. Evol. Spec. Pap. (Geological Soc. Am. https://doi.org/10.1130/SPE293-p93

Ganino, C., Libourel, G., Nakamura, A.M., Jacomet, S., Tottereau, O., Michel, P., 2018.

Impact-induced chemical fractionation as inferred from hypervelocity impact experiments with silicate projectiles and metallic targets. Meteorit. Planet. Sci. 0. https://doi.org/10.1111/maps.13131

Grossman, J.N., Rubin, A.E., MacPherson, G.J., 1988. ALH85085: a unique volatile-poor carbonaceous chondrite with possible implications for nebular fractionation processes. Earth Planet. Sci. Lett. 91, 33–54. https://doi.org/https://doi.org/10.1016/0012-821X(88)90149-5

Hamann, C., Hecht, L., Ebert, M., Wirth, R., 2013. Chemical projectile-target interaction and liquid immiscibility in impact glass from the Wabar craters, Saudi Arabia. Geochim. Cosmochim. Acta. https://doi.org/10.1016/j.gca.2013.07.030

Herbst, W., Greenwood, J.P., 2016. A new mechanism for chondrule formation: Radiative heating by hot planetesimals. Icarus. https://doi.org/10.1016/j.icarus.2015.11.026

Hughes, D.W., 1978a. Chondrule mass distribution and the Rosin and Weibull statistical functions. Earth Planet. Sci. Lett. 39, 371–376.

Hughes, D.W., 1978b. A disaggregation and thin section analysis of the size and mass distribution of the chondrules in the Bjurböle and Chainpur meteorites. Earth Planet. Sci. Lett. 38, 391–400.

Johnson, B.C., Ciesla, F.J., Dullemond, C.P., Melosh, H.J., 2018. Formation of Chondrules by Planetesimal Collisions, in: Krot, A.N., Connolly Jr., H.C., Russell, S.S. (Eds.), Chondrules: Records of Protoplanetary Disk Processes, Cambridge Planetary Science. Cambridge University Press, Cambridge, pp. 343–360. https://doi.org/DOI: 10.1017/9781108284073.013

Johnson, B.C., Melosh, H.J., 2014. Formation of melt droplets, melt fragments, and accretionary impact lapilli during a hypervelocity impact. Icarus. https://doi.org/10.1016/j.icarus.2013.10.022

520 Johnson, B.C., Minton, D.A., Melosh, H.J., Zuber, M.T., 2015. Impact jetting as the origin of
521 chondrules. Nature 517, 339.
522 Jones, A.P., Price, G.D., Price, N.J., Decarli, P.S., Clegg, R.A., 2002. Impact induced melting
523 and the development of large igneous provinces 202, 551–561.
524 Jones, R.H., Villeneuve, J., Libourel, G., 2018. Thermal Histories of Chondrules, in: Krot,
525 A.N., Connolly Jr., H.C., Russell, S.S. (Eds.), Chondrules: Records of Protoplanetary
526 Disk Processes, Cambridge Planetary Science. Cambridge University Press, Cambridge,
527 pp. 57–90. https://doi.org/DOI: 10.1017/9781108284073.003
528 Joung, M.K.R., Mac Low, M.-M., Ebel, D.S., 2004. Chondrule Formation and Protoplanetary
529 Disk Heating by Current Sheets in Nonideal Magnetohydrodynamic Turbulence.
530 Astrophys. J. https://doi.org/10.1086/381651
531 King, T.V. V, King, E.A., 1979. Size frequency distributions of fluid drop chondrules in
532 ordinary chondrites. Meteoritics 14, 91–96.
533 King, T.V. V, King, E.A., 1978. Grain size and petrography of C2 and C3 carbonaceous
534 chondrites. Meteoritics 13, 47–72.
535 Krot, A.N., Amelin, Y., Cassen, P., Meibom, A., 2005. Young chondrules in CB chondrites
536 from a giant impact in the early Solar System. Nature 436, 989.
537 Krot, A.N., Nagashima, K., Bizzarro, M., 2014. Aluminum-magnesium isotope systematics of
538 porphyritic chondrules and plagioclase fragments in CH carbonaceous chondrites, in:
539 Lunar and Planetary Science Conference. p. 2142.
540 Kruijer, T.S., Touboul, M., Fischer-Gödde, M., Bermingham, K.R., Walker, R.J., Kleine, T.,
541 2014. Protracted core formation and rapid accretion of protoplanets. Science (80-.).
542 https://doi.org/10.1126/science.1251766
543 Libourel, G., Michel, P., Delbo, M., Ganino, C., Recio-Blanco, A., de Laverny, P., Zolensky,
544 M.E., Krot, A.N., 2017. Search for primitive matter in the Solar System. Icarus 282,

375–379. https://doi.org/10.1016/j.icarus.2016.09.014

Libourel, G., Portail, M., 2018. Chondrules as direct thermochemical sensors of solar protoplanetary disk gas. Sci. Adv. 4.

Melosh, H.J., Vickery, A.M., 1991. Melt droplet formation in energetic impact events. Nature 350, 494.

Mittlefehldt, D.W., Hörz, F., See, T.H., Scott, E.R.D., Mertzman, S.A., 2005. Geochemistry of target rocks, impact-melt particles, and metallic spherules from Meteor Crater, Arizona: Empirical evidence on the impact process, in: Special Paper 384: Large Meteorite Impacts III. https://doi.org/10.1130/0-8137-2384-1.367

Mittlefehldt, D.W., See, T.H., Hörz, F., 1992. Dissemination and fractionation of projectile materials in the impact melts from Wabar Crater, Saudi Arabia. Meteoritics.

Morris, M.A., Boley, A.C., 2018. Formation of Chondrules by Shock Waves, in: Krot, A.N., Connolly Jr., H.C., Russell, S.S. (Eds.), Chondrules: Records of Protoplanetary Disk Processes, Cambridge Planetary Science. Cambridge University Press, Cambridge, pp. 375–399. https://doi.org/DOI: 10.1017/9781108284073.015

Nagahara, H., 1984. Matrices of type 3 ordinary chondrites—Primitive nebular records. Geochim. Cosmochim. Acta 48, 2581–2595.

Pilch, M., Erdman, C.A., 1987. Use of breakup time data and velocity history data to predict the maximum size of stable fragments for acceleration-induced breakup of a liquid drop. Int. J. Multiph. flow 13, 741–757.

Pilipp, W., Hartquist, T.W., Morfill, G.E., Levy, E.H., 1998. Chondrule formation by lightning in the Protosolar Nebula? Astron. Astrophys.

Rambaldi, E.R., Wasson, J.T., 1981. Metal and associated phases in Bishunpur, a highly unequilibrated ordinary chondrite. Geochim. Cosmochim. Acta 45, 1001–1015.

Rowan, L.R., Ahrens, T.J., 1994. Observations of impact-induced molten metal-silicate

570 partitioning. Earth Planet. Sci. Lett. https://doi.org/10.1016/0012-821X(94)90052-3
571 Rubin, A.E., 1989. Size-frequency distributions of chondrules in CO3 chondrites. Meteoritics
572 24, 179–189.
573 Rubin, A.E., Scott, E.R.D., Keil, K., 1982. Microchondrule-bearing clast in the Piancaldoli
574 LL3 meteorite: a new kind of type 3 chondrite and its relevance to the history of
575 chondrules. Geochim. Cosmochim. Acta 46, 1763–1776.
576 Rubin, A.E., Wasson, J.T., 2005. Non-spherical lobate chondrules in CO3.0 Y-81020:
577 General implications for the formation of low-FeO porphyritic chondrules in CO
578 chondrites. Geochim. Cosmochim. Acta. https://doi.org/10.1016/j.gca.2004.06.019
579 Ruzicka, A., Snyder, G.A., Taylor, L.A., 1998. Mega-chondrules and large, igneous-textured
580 clasts in Julesberg (L3) and other ordinary chondrites: vapor-fractionation, shock-
581 melting, and chondrule formation. Geochim. Cosmochim. Acta 62, 1419–1442.
582 https://doi.org/https://doi.org/10.1016/S0016-7037(98)00029-5
583 Saltykov, S.A., 1958. Stereometric metallography. Metall. Moscow 267.
584 Sanders, I.S., Scott, E.R.D., 2018. Making Chondrules by Splashing Molten Planetesimals, in:
585 Krot, A.N., Connolly Jr., H.C., Russell, S.S. (Eds.), Chondrules: Records of
586 Protoplanetary Disk Processes, Cambridge Planetary Science. Cambridge University
587 Press, Cambridge, pp. 361–374. https://doi.org/DOI: 10.1017/9781108284073.014
588 Scott, E.R.D., 2007. Chondrites and the protoplanetary disk. Annu. Rev. Earth Planet. Sci. 35,
589 577–620.
590 Scott, E.R.D., 1988. A new kind of primitive chondrite, Allan Hills 85085. Earth Planet. Sci.
591 Lett. 91, 1–18. https://doi.org/https://doi.org/10.1016/0012-821X(88)90147-1
592 Scott, E.R.D., Krot, A.N., 2003. Chondrites and their components. Treatise on geochemistry
593 1, 711.
594 Shu, F.H., Shang, H., Lee, T., 1996. Toward an astrophysical theory of chondrites. Science

(80-.). 271, 1545–1552.

Skinner, W.R., Leenhouts, J.M., 1993. Size distributions and aerodynamic equivalence of metal chondrules and silicate chondrules in Acfer 059, in: Lunar and Planetary Science Conference.

Teitler, S.A., Paque, J.M., Cuzzi, J.N., Hogan, R.C., 2010. Statistical tests of chondrule sorting. Meteorit. Planet. Sci. 45, 1124–1135.

Uesugi, M., Sekiya, M., Nakamura, T., 2008. Kinetic stability of a melted iron globule during chondrule formation. I. Non-rotating model. Meteorit. Planet. Sci. https://doi.org/10.1111/j.1945-5100.2008.tb00680.x

Urey, H.C., 1952. Chemical fractionation in the meteorites and the abundance of the elements. Geochim. Cosmochim. Acta 2, 269–282.

Wang, Y., Hua, X., WeiBiao, H., 2007. Petrogenesis of opaque assemblages in the Ningqiang carbonaceous chondrite. Sci. China Ser. D Earth Sci. 50, 886–896.

611 Figures:

612

613 Figure 1: (a) Aluminum witness plate and target after the impact experiment. (b) High-speed
614 video image before impact. Projectile is elongated along the trajectory due to exposure
615 duration (0.5 µs). (c) High-speed video image during the post impact blast (~14 µs after
616 impact)

617

618 Figure 2: BSE-SEM images of the aluminum ejecta catcher showing the 13 ejecta analyzed
619 (iron metal bead in white).

620

621 Figure 3: BSE-SEM images of 9 chondrules of Yamato 81020, including metal beads (in
622 white).

623 Figure 4: Cumulative size frequency of (a) chondrules in CO chondrites (data from Rubin,
624 1989 transformed into a theoretical three-dimensional size distribution after a Saltykov
625 analysis; n = 2334) ; (b) ejecta from hypervelocity experiment (n = 9326), (c) metal
626 beads in chondrules of Yamato 81020 transformed into a theoretical three-dimensional
627 size distribution after a Saltykov analysis (n = 3517; dotted line = individual analyses in
628 the nine chondrules shown in Figure 3, bold line = mean), (d) metal beads in ejecta
629 (n = 1625; dotted line = individual analyses in the thirteen ejecta shown in Figure 2, bold
630 line = mean).

631 Figure 5: Size frequency of chondrules in CO chondrules (data from Rubin, 1989 transformed
632 into a theoretical three-dimensional size distribution after a Saltykov analysis, n = 2834),
633 ejecta from hypervelocity experiment (n = 9326), metal beads in chondrules of Yamato
634 81020 transformed into a theoretical three-dimensional size distribution after a Saltykov
635 analysis (n = 3517) and metal beads in ejecta (n = 1625).

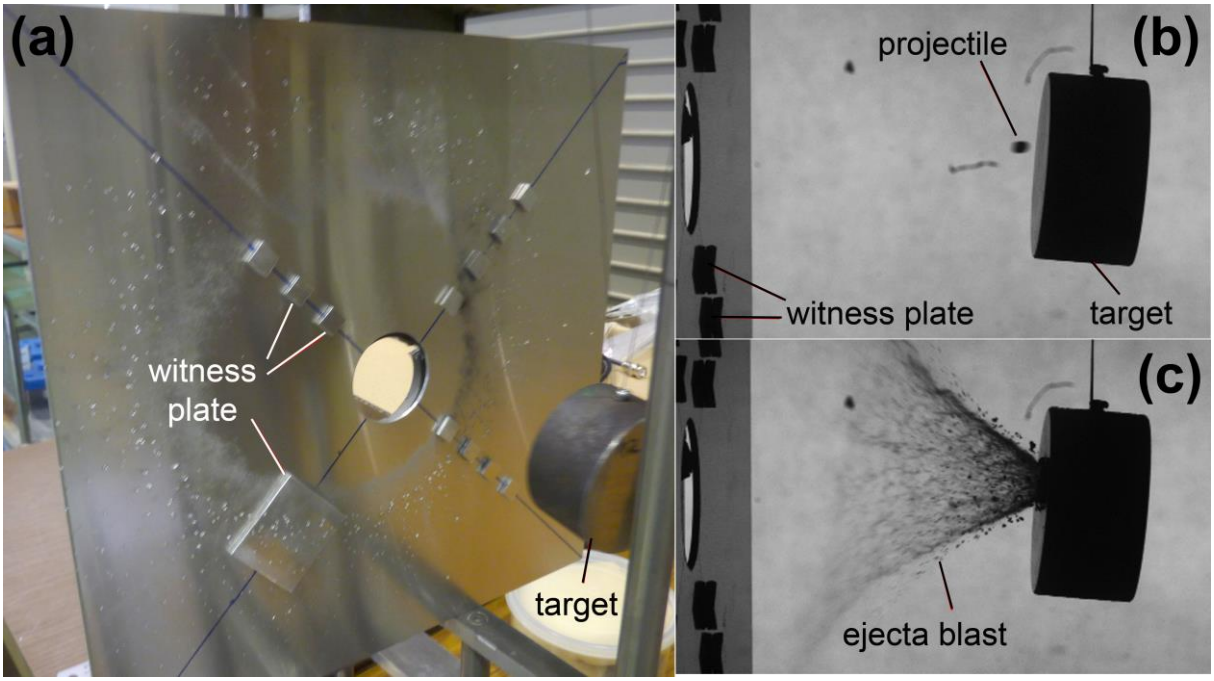
(a)
witness
plate
target
projectile
(b)
witness plate
target
(c)
ejecta blast

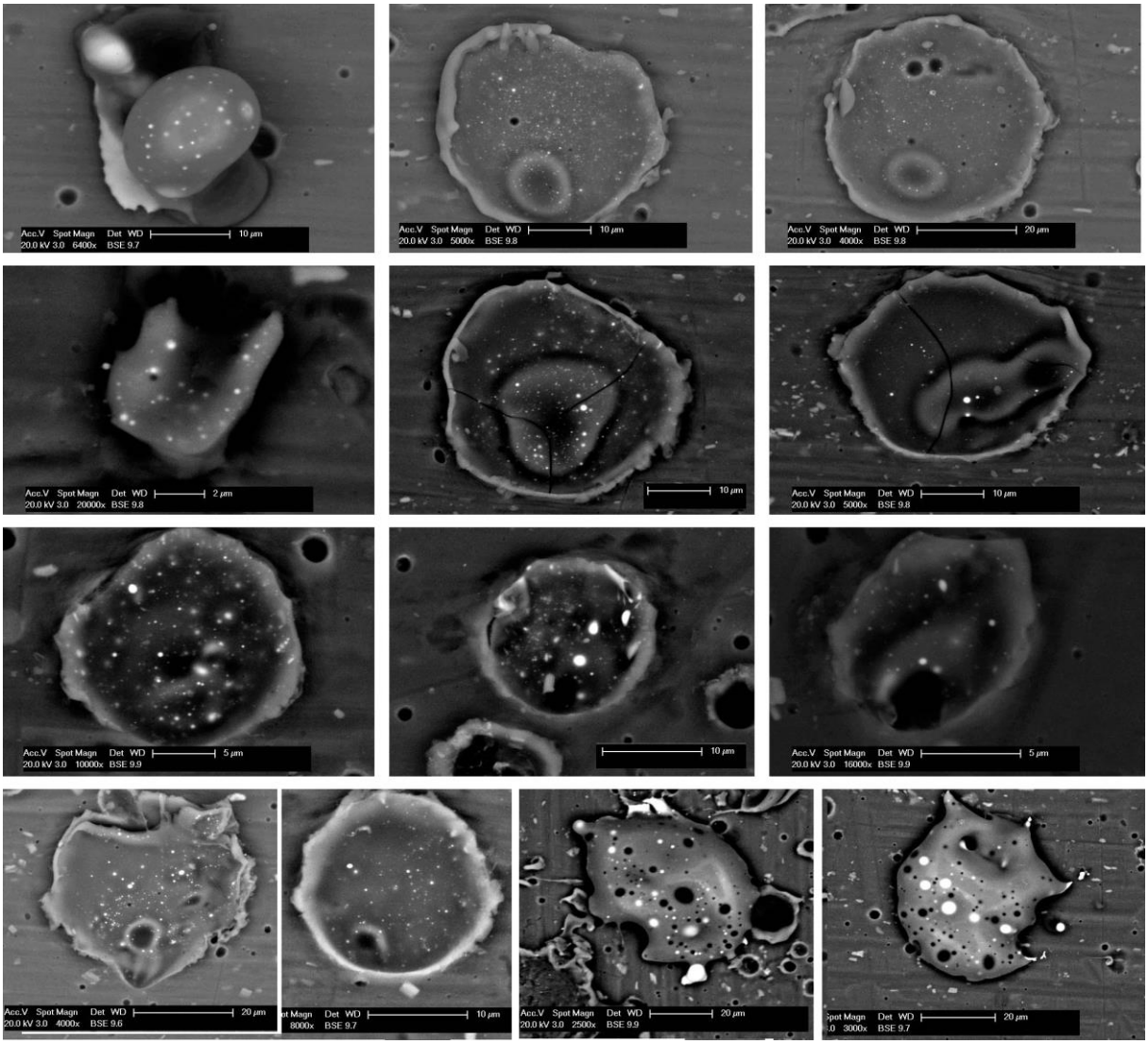
Acc.V Spot Magn Det WD 10 µm
20.0 kV 3.0 6400x BSE 9.7
Acc.V Spot Magn Det WD 10 µm
20.0 kV 3.0 5000x BSE 9.8
Acc.V Spot Magn Det WD 20 µm
20.0 kV 3.0 4000x BSE 9.8
Acc.V Spot Magn Det WD 2 µm
20.0 kV 3.0 20000x BSE 9.8
10 µm
Acc.V Spot Magn Det WD 10 µm
20.0 kV 3.0 5000x BSE 9.8
Acc.V Spot Magn Det WD 5 µm
20.0 kV 3.0 10000x BSE 9.9
10 µm
Acc.V Spot Magn Det WD 5 µm
20.0 kV 3.0 16000x BSE 9.9
Acc.V Spot Magn Det WD 20 µm
20.0 kV 3.0 4000x BSE 9.6
Det WD 10 µm
8000x BSE 9.7
Acc.V Spot Magn Det WD 20 µm
20.0 kV 3.0 2500x BSE 9.9
Det WD 20 µm
3000x BSE 9.7

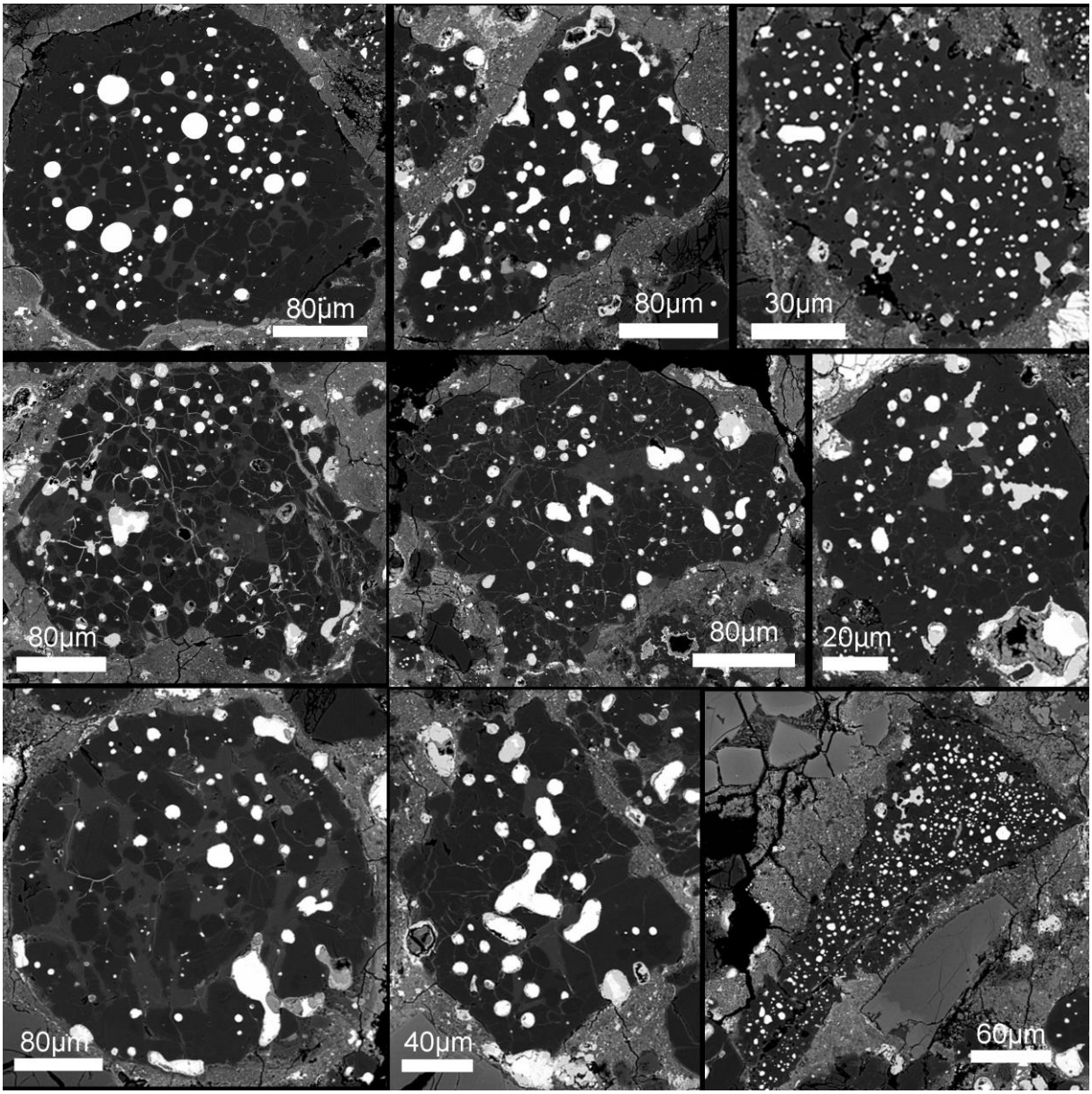
80μm
80μm
30μm
80μm
80μm
20μm
80μm
40μm
60μm

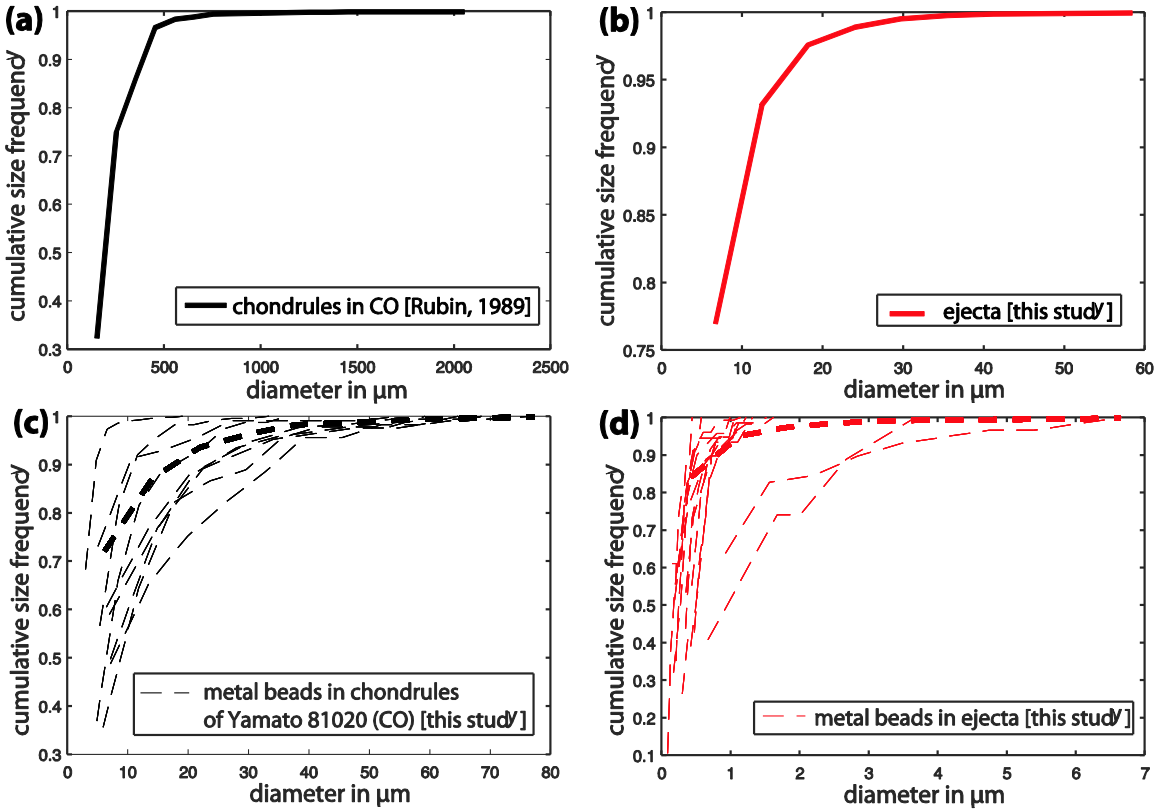
(a)
cumulative size frequency
diameter in µm
chondrules in CO [Rubin, 1989]
(b)
cumulative size frequency
diameter in µm
ejecta [this study]
(c)
cumulative size frequency
diameter in µm
metal beads in chondrules
of Yamato 81020 (CO) [this study]
(d)
cumulative size frequency
diameter in µm
metal beads in ejecta [this study]

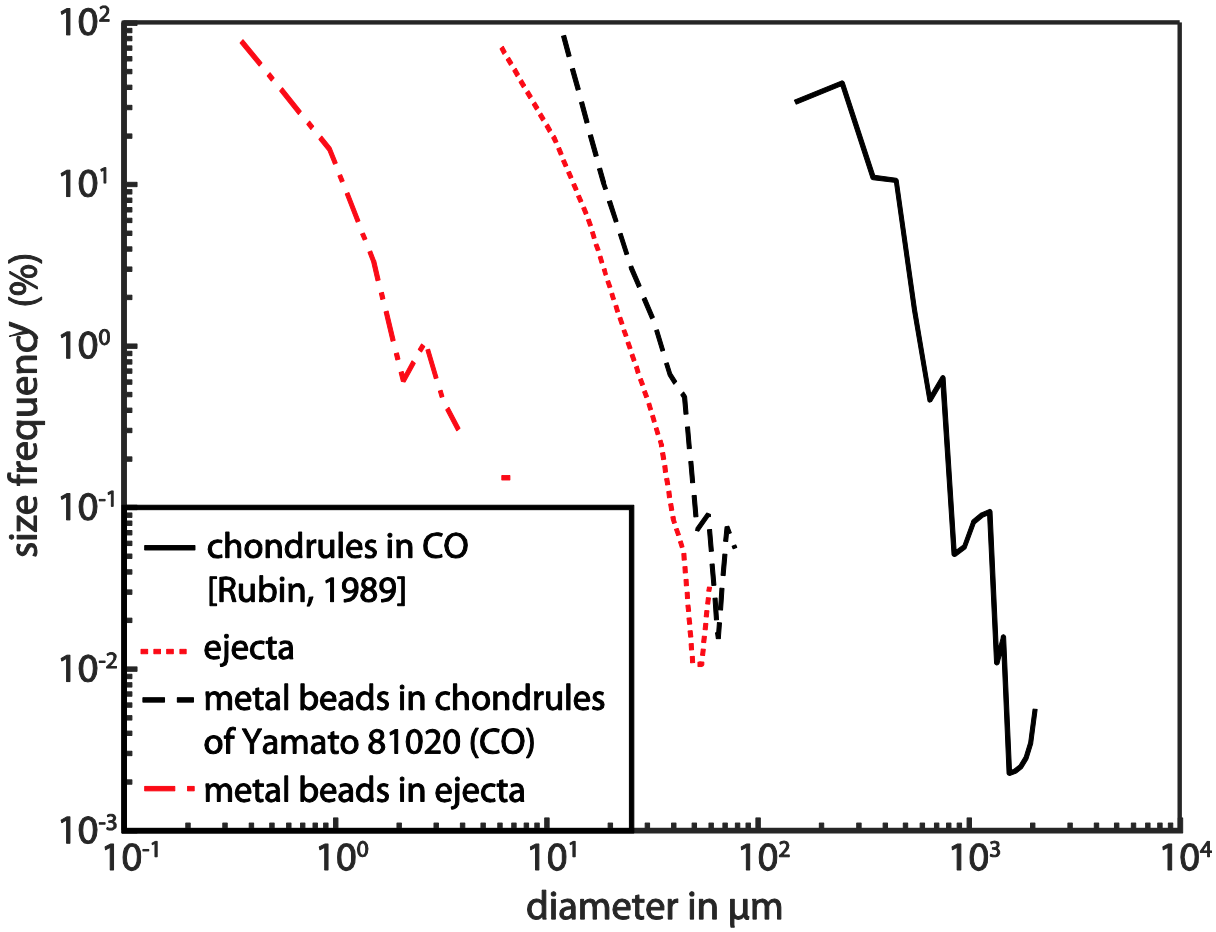
size frequency (%)
diameter in µm
chondrules in CO
[Rubin, 1989]
ejecta
metal beads in chondrules
of Yamato 81020 (CO)
metal beads in ejecta